

Precipitation in a High-strength Al-Cu-Li Alloy

Jasmine C. Shih¹, Matthew Weyland² and Barrington C. Muddle¹

¹ARC Centre of Excellence for Design in Light Metals, Department of Materials Engineering, Monash University, Victoria 3800, Australia

²Monash Centre for Electron Microscopy, Monash University, Victoria 3800, Australia

The improved properties of third generation 2xxx series Al-Cu-Li alloys, especially in terms of toughness and thermal stability, have led to their adoption in high performance aerospace applications. Described here is a preliminary study of the microstructural evolution in a representative alloy AA2199, under isothermal ageing from as-quenched (T3) condition to maximum hardness. In particular, the formation and evolution of the key strengthening precipitate, the T₁ (Al₂CuLi) phase, is characterized. The first appearance of this phase is isolated to between 1 and 4 h of ageing at 140-150°C, and the average length, and aspect ratio, of the precipitate correlated to the hardness of the alloy. Maximum hardness is achieved with a plate length of ~65 nm, corresponding to an aspect ratio of ~55:1. Observations of the early evolution of T₁ precipitates, using aberration-corrected scanning transmission electron microscopy (STEM), reveals their distribution to be non-uniform, with T₁ formation preferentially associated with a previously unreported sub-nm sized precipitate population. These precipitates, which show strong structural similarity to Guinier-Preston-Bagaryatsky (GPB) zones, form in distinctive 'ribbons', with a morphology implying that they decorate dislocations.

Keywords: *Al-Cu-Li alloys, microstructural evolution, precipitation strengthening, aberration-corrected STEM*

1. Introduction

The weight reduction achieved by the use of high specific strength aluminium alloys in modern aircraft design has led to significant improvements in fuel efficiency. The Al-Cu-Li alloy family is exceptional in this regard as 1 wt% of Li in an Al alloy reduces the density by ~3% and increases the modulus by ~6% [1]. Since the introduction of the first generation of Al-Cu-Li alloys (e.g. AA 2020) in the 1950s, this class of alloys has been used in the aerospace industry [1-3]. While early Al-Cu-Li alloys tended to have excessive anisotropy of mechanical properties, and less than desirable ductility and fracture toughness, continuous improvements in the properties have been made and the third generation alloys are found in modern aircraft, such as the Airbus A380.

In the most recent Al-Cu-Li alloys, the key to high strength is a uniform distribution of T₁ precipitates (nominal composition Al₂CuLi), which form as thin plate-shaped particles of large aspect ratio (diameter:thickness) parallel to {111}_a planes of α -Al matrix. One of the unusual, and thus far unexplained, characteristics of T₁ precipitates is that despite being near to fully coherent with an α -Al matrix, with apparently minimal misfit strain energy, they will not nucleate readily without specific conditions being fulfilled. In particular, there are two known routes to promoting uniform, fine-scale T₁ precipitation: (a) plastic deformation (typically 3-6% stretch) of the alloy prior to ageing, or (b) the combined addition of trace concentrations (0.3-0.5 wt%) of Ag and Mg to the alloy.

The present research has two clear goals. Firstly, to study the overall structural evolution of the representative Al-Cu-Li alloy AA2199 [4] though isothermal heat-treatment to maximum hardness, using conventional transmission electron microscopy (TEM). Secondly, to better understand the

factors controlling the formation of the T_1 phase, using recent generational advances in (Scanning)TEM characterization techniques.

2. Experimental Details

The composition specification of the alloy AA2199 [4] studied is provided in Table 1. The sheet received was 4mm thickness and pre heat treated to the T3 condition (solution treated, quenched and stretched to a uniform elongation of ~3%). This sheet was cut into multiple strips with dimensions of $3 \times 1 \times 0.4$ cm, and the as-received strips aged isothermally in oil baths at 140°C and 150°C for various times and water quenched. Vickers hardness measurements (VHN) from the heat-treated strips were obtained with a load of 3 kg and dwell time of 5 s. Samples aged for 1, 4, 24, 72 and 97 h at 150°C were prepared for TEM, by punching into 3 mm discs, polishing mechanically to a thickness of ~150 μm , and twin-jet electropolishing using 33 vol.% HNO_3 in methanol at a temperature of -25°C.

The general microstructural evolution, from as-received specimens to those in maximum hardness condition, was studied using bright field (BF) TEM and selected area electron diffraction (SAED) on a Philips CM20 TEM operating at 200 kV. The scale of T_1 precipitates was assessed by measuring the projected lengths of large populations of particles observed in <110> matrix orientation, with the habit plane parallel to the electron beam. Measurements were made using Digital Micrograph and, for each aging condition, over 120 individual precipitates were measured for selected, with errors reported on population averages corresponding to a standard deviation. The results reported have not been corrected for truncation effects arising from the thin foil nature of the specimens; preliminary emphasis has been on a comparative (rather than absolute) measure of average precipitate dimensions as a function of heat treatment.

Aberration-corrected scanning transmission electron microscopy (STEM) was carried out using an FEI Titan³ 80-300 FEG-(S)TEM, fitted with two CEOS aberration correctors, operated at 300 kV. A convergence angle of 15.1 mrad was used for all imaging, giving a probe size of $\leq 0.1\text{nm}$. Images were acquired with an inner collection angle of 50 mrad in atomic number Z-contrast high-angle annular dark field (HAADF) mode and at 16 mrad for strain-enhanced low-angle (LA)ADF mode.

Table 1 Composition specification of alloy AA2199

	Cu	Li	Zn	Mg	Mn	Zr	Fe	Si	Al
at.%	0.98-1.2	5.45-7.00	0.083-0.37	0.056-0.44	0.049-0.246	0.015-0.036	0.034	0.048	93.3

3. The Evolution of Hardness

The hardening response of the samples aged at 140 and 150°C are compared in Fig. 1. The as-received material had a hardness of 99 ± 3 VHN, which notably was significantly higher than that of samples exposed for the shortest ageing times at both 140 and 150°C. After just 1 h at both temperatures, the hardness had decreased to ~85 VHN. The origin of this decrease is likely to be associated with relatively rapid recovery and rearrangement within the dislocation substructure introduced during plastic deformation (3% stretch) post solution treatment. The alloy did not recover this hardness and surpass the as-received value until more than 8 h of ageing at both temperatures.

The hardness of the samples did not increase significantly until 32 h ageing at 140°C and after 16 h at 150°C. The maximum hardness for isothermal ageing at 140°C occurred at ~340 h (14 days) with a VHN of 158 ± 4 , while the maximum hardness for samples aged at 150°C was achieved at ~70 h, with a VHN of 154 ± 6 . The acceleration in the ageing response is expected at the higher

temperature and attributable to increases in the rates of solute diffusion. A reduction in maximum hardness might also be expected at the higher ageing temperature, but the difference of just 10°C in temperature is likely sufficiently small that the difference is not significant.

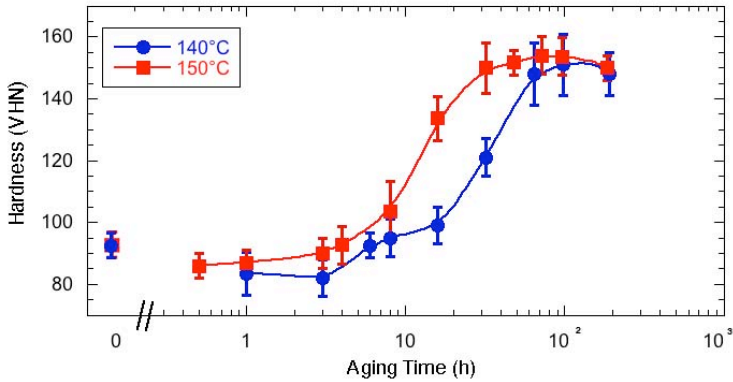


Fig. 1 Hardness curves of the alloy isothermally aged at 140°C and 150°C.

4. Microstructural Evolution

Bright field TEM and selected area electron diffraction (SAED) has been used to characterise the microstructural evolution of the alloy at selected times during isothermal aging at 150°C. TEM micrographs were taken with the electron beam along <110> directions of the Al matrix. Figure 2 shows the evolution from key points of the hardness curves.

For short ageing time (1h), Fig. 2(a), there was little evidence of precipitation detectable by either TEM or SAED, and the microstructure exhibited the strain contrast associated with a dense distribution of dislocations in cellular array. The first detectable increases in hardness were coincident with the formation of T₁ precipitates; a small number density of non-uniformly distributed T₁ was observed after 4 h aging time, localised to strained regions of the crystal and apparently primarily associated with dislocation substructure. With increasing ageing time, the number density of T₁ precipitates increased and the distribution became more uniform, Figs 2(c)-(f). At maximum hardness (VHN 154 ± 6), which occurred between 72 and 97 h at 150°C, the T₁ precipitates appeared to uniformly partition the matrix phase, Figs 2(e)-(f), while remaining associated with strain contrast that apparently signify a residual dislocation substructure. After 185 h, the alloy was beginning to overage at 150°C and initially this appears to be associated with a full recovery/annealing of the dislocation substructure.

With the exception of Fig. 2(a), the SAED patterns inset in Fig. 2 reveal precipitate reflections that can primarily be indexed for multiple variants of the T₁ phase. However, there are additional Bragg reflections likely due to small volume fractions of additional precipitate phases and, on the basis of this preliminary study, it is not possible to rule out the presence of additional metastable constituents, such as GP zones, δ', θ', and S phase and its precursors [4].

As the primary strengthening elements in the aged microstructures, the high aspect ratio T₁ precipitates partition the matrix phase to provide obstacles to dislocation motion under applied stress. The effectiveness of the precipitate distribution will be determined by a range of factors, including the scale, aspect ratio, distribution and spacing of the individual particles. Figure 3 shows selected histograms of the projected length distributions from representative aging conditions. The histograms suggest that the variation in initial T₁ size does not follow a normal distribution, and this distribution may change with heat treatment. However, this raw data has not been corrected for truncation errors that may arise from the thin foil geometry of the specimens and the sample populations are not sufficiently large to make such conclusions with full statistical significance. The average projected length is seen to increase continuously with increasing ageing time up to at least ~100 h and, in Figure 4, the average projected precipitate length is plotted against measured sample

hardness (VHN). There appears to be an approximately linear empirical correlation up to maximum hardness. At maximum hardness, the average projected precipitate length was typically in the range of ~60-70 nm and, given that the thickness of the average T_1 plate was one unit cell or $\sim 5 \times 0.24$ nm $<111>$ planes, the typical aspect ratio was of the order of 55:1 (projected length:thickness).

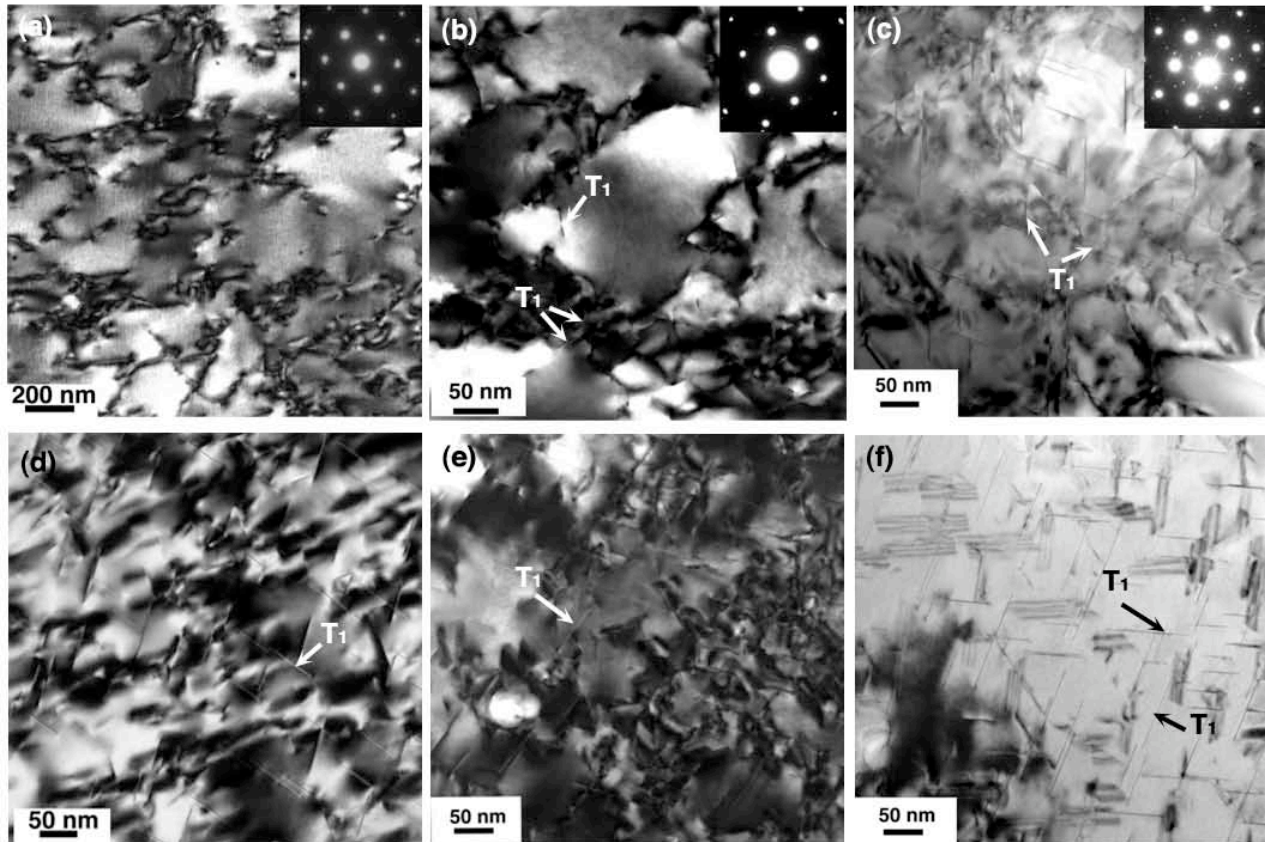


Fig. 2 BF TEM micrographs taken along $<110>$ directions in the Al matrix from selected aging times at 150°C: (a) 1 h, (b) 4 h, (c) 24 h, (d) 72 h, (e) 97 h and (f) 185 h. Inset are the SAED patterns recorded.

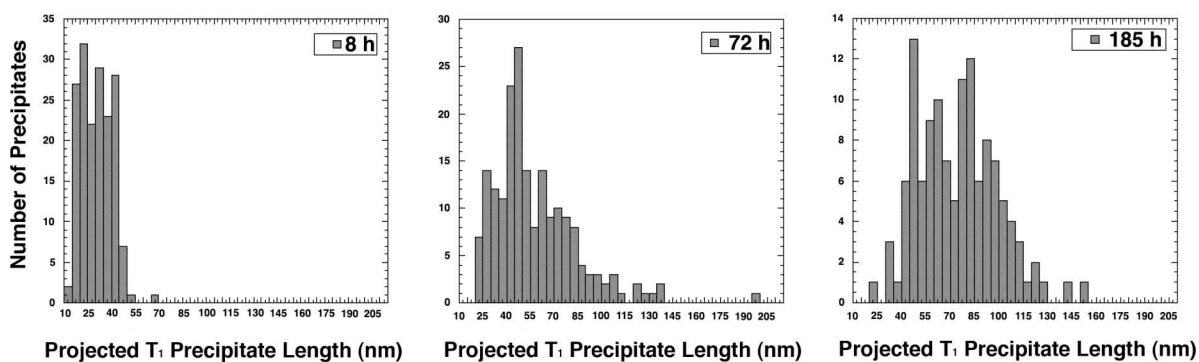


Fig. 3 Histograms of the distributions of projected lengths of T_1 precipitates measured for selected aging times at 150°C.

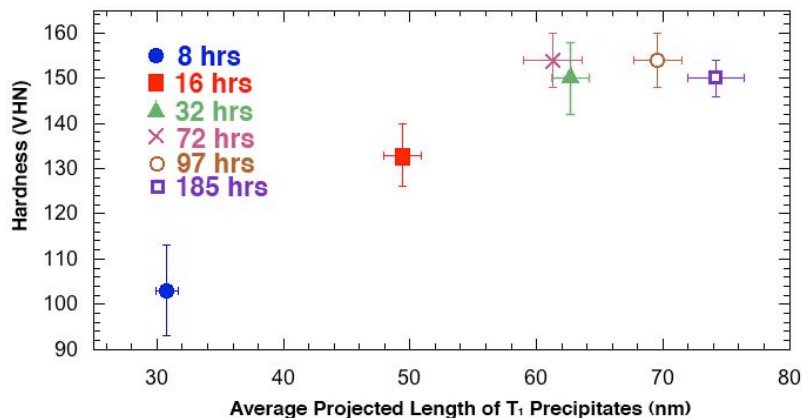


Fig. 4 Hardness versus average projected T₁ precipitate length for various ageing times at 150°C

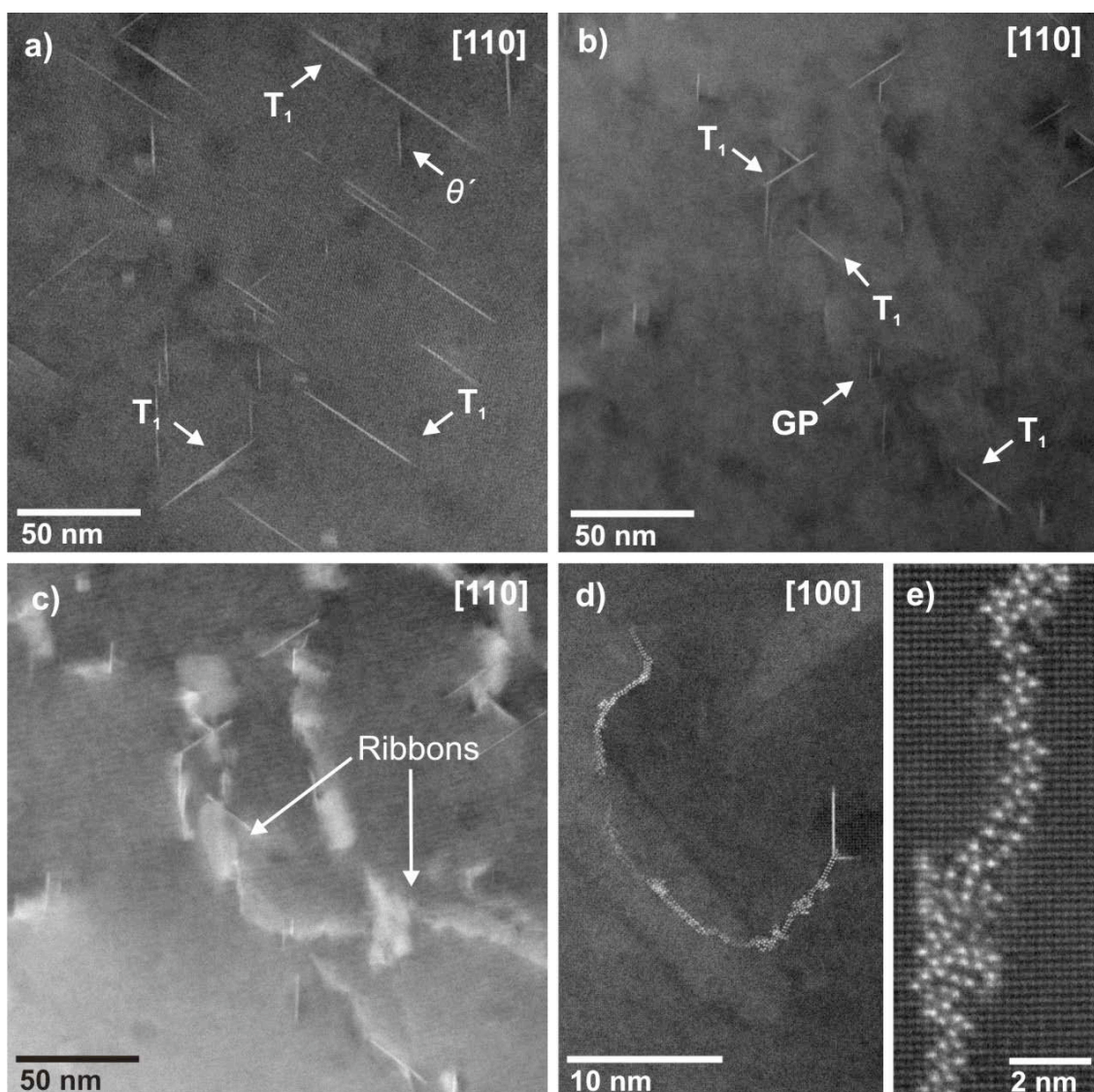


Fig. 5 HAADF STEM images from (a) 32 h ageing showing well-dispersed T₁ and other precipitates, viewed along [110]. From (b) 8 h ageing showing non-uniform T₁ distribution, and GP zones. (c) LAADF STEM image from the same area as (b) showing isolated T₁ connected by "ribbons" of confined strain contrast. (d) HAADF STEM image along a <100> direction showing ribbons edge on are complicated precipitate chains, that at high magnifications (e), show a semi-regular structure related to GPB and S phases. All samples aged at 150°C.

Observation the alloy after 32 h ageing by HAADF STEM, Fig. 5(a), shows the distinct advantages of this technique for imaging highly strained crystals when compared to BF TEM. With intensity related largely to thickness and atomic number these ‘Z-contrast’ images clearly show the well-dispersed nature of the T_1 precipitates. An observation of a specimen aged 4 h, Fig. 5 (b), shows the non-uniform distribution of T_1 at short ageing times. From the BF TEM images the T_1 at these ageing times seems to be co-incident with a network of highly strained crystal. However it is unclear what is the source of strain; dislocations or precipitates. The LAADF STEM image in Fig. 5(c), of the same area of crystal as Fig. 5(b), reveals the seemingly isolated T_1 to be connected to a network of ribbons of well-defined high strain, which shows in bright contrast in this collection geometry. When tilted to an $<001>$ direction these ribbons resolve into chains of small precipitates that form clear loops through the microstructure, Fig. 5(d). At higher magnifications, Fig. 5(e), these show a complicated crystal structure bearing similarities to GPB zones and S phase precipitates. They are also similar to those reported by Kovarik et al [5] in Al-Cu-Mg alloys.

5. Summary

A preliminary study has been made of the microstructural evolution in a typical third-generation Al-Cu-Li alloy, most notably in terms of the relationship between microstructure and hardness. It was observed that the age-hardening response is primarily correlated with formation of the T_1 phase, with precipitates becoming detectable between 1 and 4 h of ageing at 150°C. For ageing in the range of 8-100 h at 150°C, there was an approximately linear increase in hardness with increase in the average projected length of T_1 precipitate plates, with the projected length being used as an initial comparative indicator of average plate diameter and aspect ratio. In early ageing, T_1 forms an inhomogeneously dispersed population, associated with regions of high lattice strain. The use of LAADF STEM indicates that this lattice strain is confined to uniform regions. High resolution STEM results suggest that these regions are actually caused by a previously unreported ribbon like precipitates, which form along $<001>$ directions, and share structural similarities to GPB zones and S phase precipitates. These precipitates form discrete ‘loops’, suggesting they decorate the dislocations in the microstructure. Whether nucleation of T_1 is associated directly with dislocations or with metastable constituents that decorate the dislocations remains to be resolved by future application of advanced microscopy techniques.

Acknowledgements

The authors acknowledge gratefully the support of the Australian Research Council, Monash University and the Monash Centre for Electron Microscopy. The FEI Titan 80-300 FEGTEM was funded through ARC Grant LE0454166. Samples of the alloy were generously supplied by Alcoa Technical Centre, Pennsylvania, USA.

References

- [1] J.C. Williams and E.A. Starke: *Acta Mater.*, 51 (2003) 5775-5799.
- [2] A.K. Vasudévan, P.E. Bretz, and A.C. Miller: *Mater. Sci. and Eng.*, 64 (1984) 113-122.
- [3] J.G. Rinker, and M. Marek: *Mater. Sci. and Eng.*, 64 (1984), 203-221.
- [4] C. Giummera, R.J. Rioja, G.H. Bray, , P.E. Magnusen and J.P. Moran, *Aluminium Alloys: Their Physical and Mechanical Properties*, Ed. By J. Hirsch, B. Skrotzki and G. Gottstein, (Wiley-VCH, Weinheim, 2008), pp. 176-88.
- [5] L. Kovarik, S.A. Court, H.L. Fraser, and M.J. Mills: *Acta Mater.* 56(2008), 4804-4815